Anal Bioanal Chem (2011) 400:2499–2506
DOI 10.1007/s00216-011-4952-0

ORIGINAL PAPER

Surface molecular imprints of WGA lectin as artificial receptors for mass-sensitive binding studies

Thipvaree Wangchareansak · Chak Sangma · Kiattawee Choowongkomon · Franz Dickert · Peter Lieberzeit

Received: 29 October 2010 / Revised: 21 March 2011 / Accepted: 22 March 2011 / Published online: 7 April 2011

Abstract Wheat germ agglutinin (WGA) lectin is a model compound for the interaction between viruses and cells during infection events and thus an interesting analyte for mass-sensitive sensing to study these interaction phenomena. Scanning tunneling microscopy studies reveal that surface molecular imprinting leads to cavities having the dimensions of WGA dimers. These reincorporate WGA from phosphate-buffered saline between 1 and 160 μg/ml. Whereas the quartz crystal microbalance (QCM) frequency for molecularly imprinted polymer (MIP)-coated electrodes decreases, indicating uptake of the analyte, their nonimprinted counterparts yield positive, concentration-dependent frequency shifts characteristic for slip of the analyte on the QCM surface. The MIPs achieve selectivity factors towards bovine serum albumin of roughly 4 at higher protein concentrations. Brunauer-Emmett-Teller analysis reveals that binding is favored by 29 kJ/mol until the adsorption of up to ten monolayers on the MIP, whereas above this range the value is lower. Together with the binding behavior of MIP and nonimprinted polymers, this indicates that the MIP acts as a nucleus for multilayer deposition onto the surface.

Keywords Wheat germ agglutinin lectin · Molecular imprinting · Quartz crystal microbalance · Brunauer–Emmett–Teller analysis

Published in the special issue *Analytical Sciences in Austria* with Guest Editors G. Allmaier, W. Buchberger and K. Francesconi.

T. Wangchareansak · F. Dickert · P. Lieberzeit (✉)
University of Vienna, Department of Analytical Chemistry,
Waehringer Strasse 38,
1090 Vienna, Austria
e-mail: peter.lieberzeit@univie.ac.at

T. Wangchareansak · C. Sangma
Department of Chemistry, Faculty of Science,
Kasetsart University,
Chatuchak,
Bangkok 10900, Thailand

K. Choowongkomon
Department of Biochemistry, Faculty of Science,
Kasetsart University,
Chatuchak,
Bangkok 10900, Thailand

Introduction

Lectins are large glycoproteins which can be found in a wide range of biological systems, such as viruses, plants, fungi, yeasts, bacteria, and animals [1]. They, for example, play a fundamental role in recognition processes occurring during infection of such cells by viruses: The latter bind to the carbohydrate moieties of glycoconjugates on the cell surface of the respective host [2–4]. These properties can be used for analytical and diagnostic purposes. Lectins hence play important roles in medicine, clinics, and biosensors. Owing to their ubiquity and their binding characteristics, lectins can be used as model species to investigate mechanisms of glycoprotein binding. For this purpose, a variety of detection methods have already been reported: some are based on binding of the lectin to sugar moieties detected, e.g., by a quartz crystal microbalance (QCM) [3–8], surface plasmon resonance [9–12], and electrochemical transduction [13–16]. As preparing the natural glycosidic receptor for lectin is a rather tedious, synthetically elaborate, and long-term effort, we aim at detecting the lectins themselves with molecularly imprinted polymers (MIP) and comparing their binding properties with those of analogues of the respective natural receptor.

Among other applications, molecular imprinting has attracted substantial interest in the area of selective biospecies

incorporation, as could be shown, for example, for DNA [17, 18], peptides [19, 20], cells [21], viruses [22], and proteins [23–25]. MIP in those cases function as artificial receptors by offering the respective template species a preformed, noncovalent interaction network. In the case of protein-selective cavities, stamping methods have proven most suitable. Generally speaking, imprinting consists of synthesizing a highly cross-linked polymer in the presence of the analyte-to-be or a suitable model compound. After the biotemplate species has been removed, unique cavities depicting their shape are left behind on the surface generated. The main advantages of using the surface imprinting technique are the reduction of the amount of protein template and avoidance of problems associated with template solubility in the monomer/cross-linker solution. A different approach has been reported by Miyata et al. [26], who produced acrylate/acrylamide-based hydrogels in the presence of concavalin A selectively binding the template in a type of "induced fit" reaction.

The kinetic adsorption of protein can be explained by different models, including the Langmuir, Freundlich, or Brunauer–Emmett–Teller (BET) isotherms. For small molecules, viruses, or proteins, usually the Freundlich isotherm is proposed to describe their interaction with MIP [27]. In cases where the Freundlich model is not valid, the BET isotherm for a liquid [28] phase can be applied to describe the system. Usually, the BET model is applied to describe the adsorption of gases on porous materials assuming multilayer deposition [29]. The associated BET equation can be derived by considering the differences in energy according to the Boltzmann exponential factor $\exp(-\Delta E/RT)$, the interaction energy ΔE, the thermal energy RT, and the exchange rates between sites. However, when applying the BET equation to the adsorption of proteins from liquid phase, one has to replace the partial pressure of the gas, p, by the protein concentration in solution, c. Attention has to be paid when replacing the saturation vapor pressure of the gas, p_0, with the corresponding term in the liquid phase. In the classical BET isotherm, p_0 denotes the surface saturation partial pressure in the gas phase. For protein adsorption we have replaced it by the maximum possible monolayer protein concentration on the surface, c_0, to utilize the BET equation in the liquid phase. Linearization leads to the following expression:

$$\frac{c}{n(c_0 - c)} = \frac{1}{n_m b} + \frac{b-1}{n_m b}\left(\frac{c}{c_0}\right). \quad (1)$$

The number of adsorbed proteins in the sensitive layer (n) can be derived from the frequency shift of the sensor. The QCM sensitivity can be calculated from the Sauerbrey equation (Eq. 2) and corresponds to 4.61 Hz/ng.

$$\Delta f = -\frac{2f_0^2}{A\sqrt{\rho_q \mu_q}}\Delta m \quad (2)$$

The parameter n_m describes the number of favorable sites in the layer. The parameter b is given as

$$b = \exp\left(\frac{\Delta E}{RT}\right), \quad (3)$$

where ΔE is the difference between interaction energies of favorable and less-favorable binding sites.

Experimental

Chemicals and reagents

Wheat germ agglutinin (WGA; a lectin) and bovine serum albumin (BSA) were purchased from Sigma-Aldrich. All other chemicals were purchased from Merck, Sigma-Aldrich, and Alfa Aesar as analytical grade or the highest available synthetic grade and were used without further purification.

Polymer synthesis

For synthesizing the copolymer, we used 8.6 mg of acrylamide, 7.2 mg of methacrylic acid, and 6 mg of methylmethacrylate as the monomers and 48 mg of *N,N′*-(1,2-dihydroxyethylene) bisacrylamide as the cross-linker. We dissolved those components together with 1 mg of 2,2′-azobis(isobutyronitrile) as the initiator in 300 μl of dimethyl sulfoxide. This was then followed by prepolymerization at 70 °C for 1 h until the gel point was approached. In parallel, we prepared the template stamps by immobilizing WGA on glass substrates by sedimentation from phosphate-buffered saline (PBS; pH 7.4): 5 μl of WGA was drop-coated onto 5×5 mm^2 glass plates. Then, we kept the coated substrate at 4 °C for 30 min, followed by spinning off the stamp at 3,000 rpm to remove excess solution and to avoid buffer recrystallization. Afterwards, we spin-coated the prepolymer mixture onto the QCM. For this purpose, we dropped 5 μl of the mixture onto the respective electrode and then spun it off at 3,000 rpm to obtain a thin layer in the range of 250–350-nm thickness. Immediately after this, we pressed the stamp onto the polymer and left it to polymerize overnight under UV light at 254 nm. To remove the template, the QCM was finally stirred in water at room temperature for 2 h. This resulted in rigid, hardly swellable polymers that can readily be applied as sensor coatings for the QCM.

QCM preparation

The electrodes were generated on AT-cut quartz wafer of 15.5-mm diameter and 168-μm thickness using a screen-printing procedure as described in previous work [30]. The resulting 10-MHz QCM were measured in a custom-made measuring cell of 80-μl volume cast from poly(dimethylsiloxane) operated in stopped-flow mode at room temperature. The QCM electrodes were connected to an oscillator circuit and this was connected to a frequency counter (Agilent 53131A) read out by a custom-made LabView routine via a GPIB USB interface. A typical measurement cycle consisted of filling the cell with PBS (10 mM, pH 7.4) and waiting for the frequency signal to reach a constant value. Then, we removed the PBS and flushed the cell with 100 μl of the respective sample solution. After this, we filled the measuring chamber with the sample and restarted recording the frequency. After the sensors had reached the equilibrium value, recording was halted again, followed by flushing the chamber twice with a cleaning solution containing 10% sodium dodecyl sulfate and 10% acetic acid in water followed by washing three times with PBS (the procedure follows that described by Pei et al. [5]). Finally, we filled the cell with PBS and restarted recording the frequency.

Scanning tunneling microscope measurement

All images were recorded with a Veeco Nanoscope IVa operated in scanning tunneling microscope (STM) mode. Prior to obtaining the images, we generated a conductive surface by sputtering both MIP and their nonimprinted counterparts with approximately 40 nm of gold in a Cressington 208HR Turbo Sputter. This is a magnetron-based system allowing for process pressures of 0.02 mbar. These are rather low values, which leads to homogeneous distribution of the target metal in the vacuum chamber. In combination with the planetary rotation of the sample head, the system is optimized to ensure absolutely uniform coating of the specimens—those introduced into the sputtering chamber. One can thus assume with certain confidence that surface structures present in the initial sample are thus readily reproduced in the final film. The STM measuring parameters were a voltage bias of 500 mV and a current set point of 50 pA.

Results and discussion

STM analysis of the imprinted surface

Generally, the first step in investigating imprinting strategies especially for biospecies consists in verifying that indeed patterns have been generated on the surface. For proteins, this poses substantial challenges owing to their size, which is usually below the resolution limit of atomic force microscopy. To achieve the necessary lateral resolution, we applied scanning tunneling microscopy. The required electrical surface conductivity was achieved by sputtering roughly 40 nm of gold onto the methacrylate. Although some similarities can be seen, the two STM images reveal distinct differences between the imprinted surface and its nontemplated counterpart. As can be seen in Fig. 1a, the nonimprinted polymer (NIP) surface is granular with narrow, steep ridges between individual polymer granules that are about 30 nm in diameter. In contrast to this, the MIP surface as depicted in Fig. 1b contains distinct cavities ranging from roughly 14 to 28 nm in diameter, some of which are marked by circles in the figure. The smallest cavities are also the narrowest (as can be seen in the cross section, Fig. 1c) and were obviously caused by a single lectin molecule standing out of the stamp surface. The cavity dimensions relate very well to the facts that WGA lectin normally exists both in its monomeric form and in its dimeric form and that the individual molecule has a mass of 36 kDa and measures approximately 14 nm × 9 nm × 4.5 nm. We obtained these dimensions by modeling published lectin structures [31] with the tools provided by the Protein Data Bank Europe (http://www.ebi.ac.uk/pdbe/). Dimensions of cavities not exactly fitting the theoretical size resulted from stamp preparation: we did not optimize it to achieve a monolayer of template. Partial multilayer adsorption of course may lead to structures that are larger than an individual molecule. Further differences between the two materials are revealed by section analysis in Fig. 1c: in the case of the NIP (lower plot), the maximum vertical difference is 4 nm. Deeper cavities (up to 4 nm) are steep and not more than 10 nm wide. On the other hand, the MIP surface reveals patterns that are up to 9 nm deep and roughly 20–25 nm wide, hence ideally matching the expected dimensions of dimeric lectins, which according to [5] is one of the two forms in which WGA can be found. Therefore, the difference between the two polymer surfaces is evident. Both the wider cavities and the substantially increased deepness within the MIP strongly indicate that the templating procedure was successful. Summarizing, to the best of our knowledge, Fig. 1 shows one of the first successful attempts to visualize imprinted cavities resulting from a protein as the template.

QCM investigation

Having obtained evidence for the presence of surface cavities, the next step is to assess the binding abilities of the resulting structures. For this purpose, we exposed dual-channel QCM coated with MIP and NIP, respectively, to different concentrations of WGA lectin in PBS (pH.7.4);

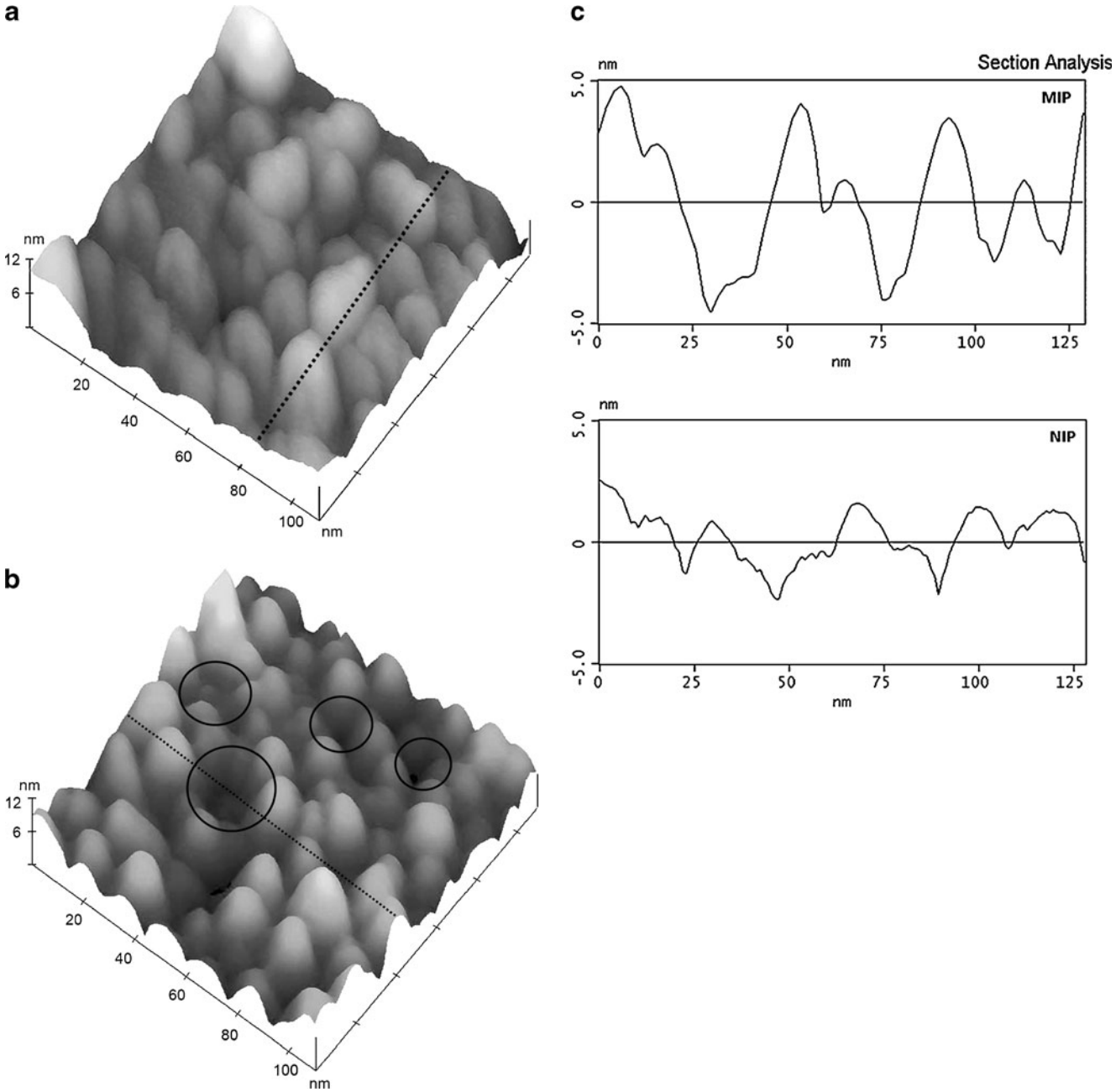

Fig. 1 Scanning tunneling microscope image with V_{bias}=500 mV and $I_{set\ point}$=50 pA. **a** Nonimprinted polymer (*NIP*; reference electrode) and **b** wheat germ agglutinin (WGA) imprinted on methacrylate copolymer. *Circles* indicate WGA imprinted cavities and *dashed lines* indicate the traces used for section analysis. **c** Section analysis for NIP (*bottom*) and WGA molecularly imprinted polymer (*MIP*; *top*) along the lines drawn in **a** and **b**

the results are shown in Fig. 2. After a short tuning period of 10 min to ensure frequency stability of the QCM, the device was exposed to WGA lectin at a concentration of 160 μg/ml. Immediately, one can observe a frequency decrease of 1,400 Hz on the MIP electrode, whereas the signal on the NIP electrode is increased by 1,025 Hz. Both effects can be reverted by washing the electrodes with sodium dodecyl sulfate/acetic acid (which leads to the dynamic response behavior of the QCM after the WGA has been removed) and also depend on the analyte concentration. In principle, this is a strong indicator of successful imprinting, because the frequency decrease on the MIP electrode is a result of mass uptake into the material. Furthermore, noise levels both in solvent and upon exposure to the protein solution remain appreciably low (in the range of 10 Hz). Therefore, one can exclude significant swelling or relaxation of the polymer matrix, because they would lead to increased damping. When this

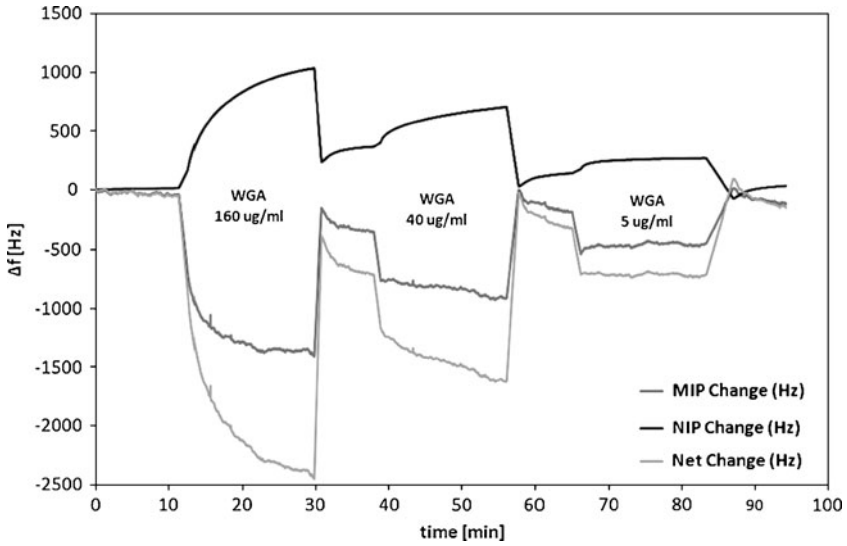

Fig. 2 Quartz crystal microbalance (QCM) sensor responses of MIP and NIP towards different WGA concentrations at 25 °C

occurs, the electronic quality factor of the device decreases, which of course directly influences the signal obtained. The frequency shifts on the NIP-coated channel, however, are positive and thus do not follow the Sauerbrey behavior that a mass increase on the electrode of a QCM leads to decreasing frequency. One of the fundamental assumptions of Sauerbrey, however, is that the additional mass on the device surface forms an ideally rigid layer unconditionally following the shear motion without viscoelastic components. Hence, the opposite behavior of WGA on the nonimprinted surface indicates that this assumption is not valid and hence only weak interaction between the individual protein molecules and the polymer surface is present. Such positive effects on QCM can also be observed with other biological species, such as yeasts and viruses [32, 33]. A systematic study by Lucklum et al. [34] suggests that the slip caused by free mobility of the device under the bioparticle leads to viscoelastic phenomena resulting in increased device frequencies. When a macroscopic analogue is used to describe this phenomenon, individual molecules can be regarded as being balls (albeit distorted in shape) on a flat, smooth surface. When this surface starts to oscillate laterally, the balls do not follow the motion, but start rolling on the surface because of their inertia.

More light can be shed on these phenomena by taking into account the selectivity of the WGA MIP and their nonimprinted counterparts. As already mentioned, WGA lectin can be applied as a model compound for assessing protein–glycoprotein binding, which plays a fundamental role in infection processes that, of course, occur on outer cell membranes surrounded by serum. Therefore, it makes sense to assess our "artificial receptors" in regard of their cross-sensitivity against serum proteins. Consequently, we applied BSA as a competing analyte, as it belongs to a class of compounds ubiquitously present in mammalian sera and has a size similar [35] to that of WGA (14 nm×4 nm×4 nm, so in one dimension it is only half as large). Figure 3 gives the frequency responses of MIP and NIP towards three different concentrations of BSA. Again, the imprinted channel undergoes a frequency decrease on exposure, whereas the nonimprinted one gives rise to positive frequency shifts in analogy to those observed for WGA. Hence, both proteins show similar behavior towards the flat, nontemplated surface. Obviously, the effects for BSA are smaller than those for WGA (as would be expected because of it smaller size, if the affinities towards the polymer are similar), but also depend on protein concentration, even though saturation of the signal can be observed. However, BSA leads to not more than half as large effects as WGA. The reason may be both the difference in size between the two species and somewhat different nonspecific interaction behavior with the polymer surface.

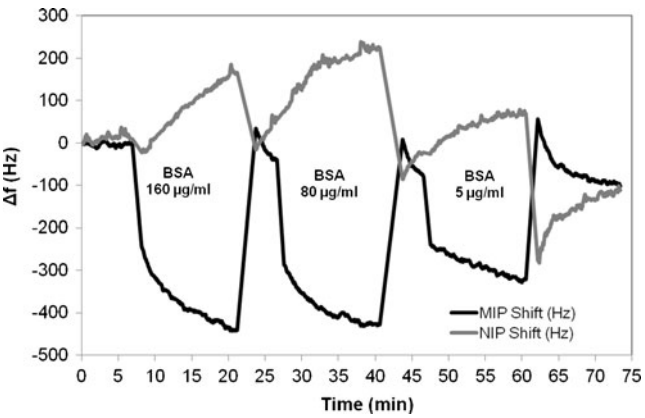

Fig. 3 QCM sensor responses of MIP and NIP towards different bovine serum albumin (*BSA*) concentrations at 25 °C

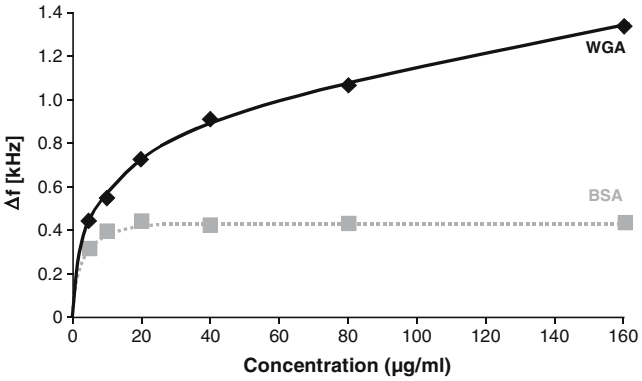

Fig. 4 The 10-MHz QCM sensor characteristics of WGA and BSA at 25 °C

The MIP, however, again shows negative, Sauerbrey-type frequency shifts, but in all cases they are smaller than those for WGA. This still leaves open the question of why no anti-Sauerbrey behavior was observed. The reason is obviously that BSA is to some extent incorporated into the cavities of the MIP, where it is not optimally bound. Still, the mobility of individual molecules on the surface and thus rolling are sufficiently hindered by the individual molecules being confined within a cavity. Summarizing, WGA lectin is tightly bound within the MIP cavities and thus follows the oscillating motion, leading to the frequency decrease, which is only true to a substantially lower extent for BSA, showing the appreciable selectivity of the system. This is not the case for the NIP, where unhindered mobility of the protein gives rise to non-Sauerbrey effects. This is even more appreciable given the fact that the conformation of the lectin on the stamp surface does not necessarily have to match the conformation in solution. However, we observed similar phenomena, for example, with insulin, where even imprinting with crystals leads to the desired results [36]. Furthermore, the frequencies of both electrodes immediately respond to the onsets of analyte exposures and depend on the concentration of WGA lectin. Therefore, this difference, in principle, can be used for quantification purposes in the given concentration range.

Interaction isotherm—binding properties

The full sensor characteristic of the system for WGA and BSA concentrations is depicted in Fig. 4. The sensor characteristic obtained for WGA shows that after a first dynamic range, the sensor signal continuously increases without reaching saturation or convergence in the respective concentration range. Similar behavior was also observed for picornaviruses in a previous study [37], where the findings suggested BET-like adsorption behavior with multilayer adsorption onto the electrode surfaces. Owing to the similarity in the dimensions of those viruses (their diameter is 30 nm) and WGA lectin, we assumed modified BET-like behavior for the WGA-imprinted layers following the arguments in that article. The outcome of the calculation is depicted in Fig. 5 after applying Eq. 1 to the QCM sensor characteristic as seen in Fig. 4. It plots the quotient of the actual solution concentration and the maximum surface concentration on the layer against the different surface concentrations at the equilibrium of each concentration. Then, n_m and b can be calculated from the intercept and the slope of the resulting straight line. The results of the initial calculations (dashed line in Fig. 5) are summarized in Table 1. The number of favorable binding sites n_m can be derived as 5×10^{12}. From b and the Boltzmann exponential factor in Eq. 3, the energy difference between favorable and unfavorable binding sites in the MIP layer is 22.2 kJ/mol. At the high concentration (160 μg/ml, -1,341 Hz), the number

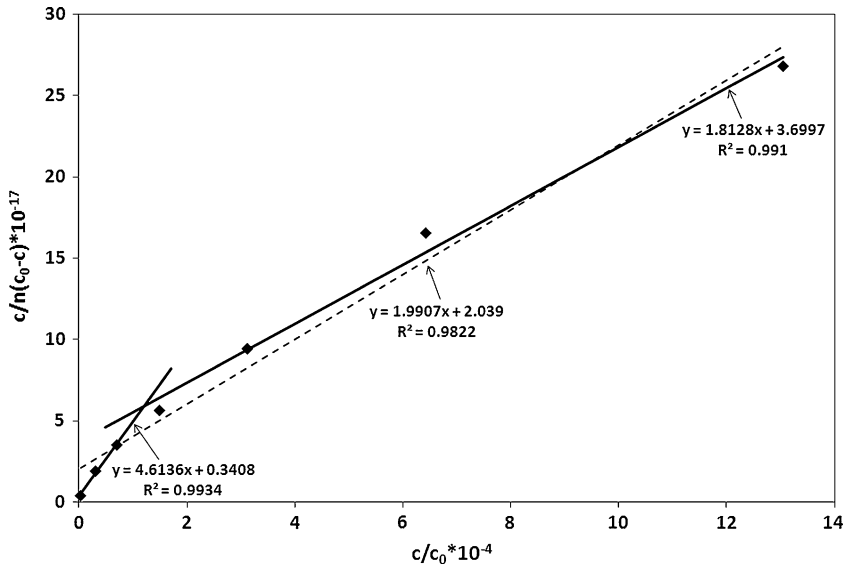

Fig. 5 Linearized Brunauer–Emmett–Teller adsorption isotherm of WGA lectin according to Eq. 1. The *dashed line* represents the overall adsorption behavior of WGA lectin with R^2=0.98, whereas the *solid lines* represent two adsorption behaviors at high and low concentration with R^2=0.99

Table 1 Calculated value for each parameter from Fig. 5 and Eqs. 1 and 3

Parameter	BET one range	BET two ranges	
		Low concentration	High concentration
n_m	5.02×10^{12}	2.17×10^{12}	5.51×10^{12}
b	7,744.60	135,376.59	4,900.86
ΔE (kJ/mol)	22.19	29.28	21.05
R^2	0.98	0.99	0.99

BET Brunauer–Emmett–Teller

of proteins bound on the surface is 4.86×10^{12}, which corresponds to roughly 97% of the available favorable binding sites, whereas it is 7.83×10^{12} at low concentration (1 μg/ml, -216 Hz), which corresponds to 16% of the available favorable binding sites. Comparing the residues between modeled and the actual data, however, reveals systematic deviations from linearity that cannot simply be disregarded.

Therefore, in a first approximation we split the data into two different concentration ranges and applied the modified BET model to them individually. Again, compared with the viruses, this approach seems valid regarding the amount of material adsorbed by the sensor: whereas for human rhinovirus, even the highest concentrations lead to less than a monolayer being deposited on the surface, the responses in this case (e.g., Δf=−1,340 Hz for 160 μg/l) clearly suggest multilayer adsorption. Table 2 summarizes the number of WGA layers adsorbed on average for each solution concentration. Multilayer adsorption can be seen even at the lowest concentration used during QCM measurements. In contrast to this, no binding can be observed on the respective nonimprinted surface. This supports the explanation that the imprinting process is necessary to bind protein onto the surface. These occupied MIP binding sites may then work as "crystallization seeds" for further protein adsorption, a phenomenon that was observed in earlier studies on lysozyme MIP [38].

In contrast to this, the BSA binding isotherm shows very early saturation of the signal, indicating that the amount cross-sensitivity is limited. Together with the fact that the MIP channels show Sauerbrey effects for both analytes, it is evident that structuring a polymer surface itself in the correct size range increases its binding ability towards proteins. However, the substantial differences in the binding isotherms also indicate that functional groups on the surface also play a seminal role in selective binding. In terms of further sensor application, it also shows that the influence of serum protein on the sensor signal remains constant above a threshold value. This shows that the sensors, in principle, can be tuned towards application in real-life serum conditions.

Generally speaking, the BET curve obtained for WGA allows one to derive two different binding ranges on the QCM: one where cavities of the MIP surface are still exposed to the solution and thus are unoccupied and a second one where this is no longer the case, but new layers are deposited on the quartz surface anyway. When this double linear model (for detailed results see Table 1) is applied in the low concentration range (1–10 μg/ml), n_m= 2.17×10^{12} and ΔE=29.3 kJ/mol. For high concentration (20–160 μg/ml), n_m=5.51×10^{12} and ΔE=21.05 kJ/mol. In both cases, the correlation coefficient is as high as 0.99 and therefore substantially better than in the single linear model. In the low concentration range, the energy difference between favorable and unfavorable binding sites corresponds to roughly three hydrogen bonds per protein molecule, which is a reasonable figure given the dimensions of the individual proteins. As already mentioned, this behavior can be explained by the MIP acting as a "crystallization catalyst" for proteins: binding to the MIP surface is favored over protein–protein agglutination (and it is known that WGA tends to agglutinate and form dimers, trimers, and tetramers [31]). Therefore, the MIP binds WGA in its cavities. Those immobilized molecules are then the "seeds" for further protein crystallization, leading to the constant increase of sensor signal with increasing solution concentration. After ten layers have been adsorbed on the QCM surface, all favorable binding sites in the MIP are occupied. Further adsorption is thus defined by intermolecular interactions between individual WGA lectins, leading to a somewhat lower binding ability and a slightly reduced energy difference between the different types of interaction sites. On

Table 2 Correlation between wheat germ agglutinin (*WGA*) lectin concentration and number of adsorbed WGA monolayers on a 10-MHz quartz crystal microbalance

WGA concentration (μg/ml)	Number of monolayers
160	25
80	20
40	17
20	13
10	10
5	8
1	4

the other hand, the nonimprinted surface is not able to immobilize individual WGA (or BSA) molecules. These remain mobile—as can be seen from the non-Sauerbrey effects in Fig. 2—and thus in terms of protein crystallization behave similarly as in solution. Generally, this also shows that imprinting leads to strong enthalpic favoring of adsorption, whereas the NIP at least disfavors it.

Conclusion

Surface molecular imprinting leads to surface interaction sites whose dimensions are determined by the size of WGA lectin dimers. The resulting materials can be characterized by scanning tunneling microscopy after sputtering and lead to selective and sensitive chemical sensing of the analyte protein when it is applied as recognition films on QCM. The advantage of this technique is real-time detection. Selectivity studies with BSA show that the resulting cavities also discriminate the proteins by surface chemistry. Overall, MIP are stable at room temperature and neutral pH. They can be applied without significant losses of sensitivity and selectivity at least for 3 weeks. Studies on the WGA–MIP adsorption behavior suggest that the MIP itself works as a "crystallizing nucleus" for the protein, even though the nonimprinted material disfavors WGA adsorption. This can be seen by the fact that up to 25 monolayers of protein are deposited on the MIP in the observed concentration range, whereas the NIP-coated electrodes yield positive frequency shifts indicating anti-Sauerbrey behavior.

Acknowledgements Financial support by the Royal Golden Jubilee Grant Foundation, the Thai Research Fund (TRF), Bilateral Research Cooperation (BRC), Faculty of Science, Kasetsart University, and ASEA UNINET is gratefully acknowledged.

References

1. Loris R, Hamelryck T, Bouckaert J, Wyns L (1998) Biochim Biophys Acta Protein Struct Mol Enzymol 1383:9–36
2. Ni Y, Tizard I (1996) Vet Immunol Immunopathol 55:205–223
3. Safina G, van Lier M, Danielsson B (2008) Talanta 77:468–472
4. Shen ZH, Huang MC, Xiao CD, Zhang Y, Zeng XQ, Wang PG (2007) Anal Chem 79:2312–2319
5. Pei Z, Anderson H, Aastrup T, Ramstrom O (2005) Biosens Bioelectron 21:60–66
6. Pedroso MM, Watanabe AM, Roque-Barreira MC, Bueno PR, Faria RC (2008) Microchem J 89:153–158
7. Pei YX, Yu H, Pei ZC, Theurer M, Ammer C, Andre S, Gabius HJ, Yan MD, Ramstrom O (2007) Anal Chem 79:6897–6902
8. Radulescu MC, Bucur B, Bucur MP, Radu GL (2009) Eur Food Res Technol 229:833–840
9. Wilczewski M, Van der Heyden A, Renaudet O, Dumy P, Coche-Guerente L, Labbe P (2008) Org Biomol Chem 6:1114–1122
10. Foley KJ, Forzani E, Tao N, Joshi L (2006) Glycobiology 16:1156–1156
11. Murthy BN, Sinha S, Surolia A, Indi SS, Jayaraman N (2008) Glycoconj J 25:313–321
12. Vornholt W, Hartmann M, Keusgen M (2007) Biosens Bioelectron 22:2983–2988
13. Hone DC, Haines AH, Russell DA (2003) Langmuir 19:7141–7144
14. Sadik OA, Yan F (2007) Anal Chim Acta 588:292–296
15. Oliveira MDL, Correia MTS, Coelho LCBB, Diniz FB (2008) Colloids Surf B 66:13–19
16. Sugawara K, Kamiya N, Hirabayashi G, Kuramitz H (2007) Talanta 72:1123–1128
17. Spivak DA, Shea KJ (2001) Anal Chim Acta 435:65–74
18. Liang HJ, Angelini TE, Ho J, Braun PV, Wong GCL (2003) J Am Chem Soc 125:11786–11787
19. Janiak DS, Kofinas P (2007) Anal Bioanal Chem 389:399–404
20. Hart BR, Shea KJ (2002) Macromolecules 35:6192–6201
21. Seifner A, Lieberzeit P, Jungbauer C, Dickert FL (2009) Anal Chim Acta 651:215–219
22. Bolisay LD, Culver JN, Kofinas P (2007) Biomacromolecules 8:3893–3899
23. Bossi A, Bonini F, Turner APF, Piletsky SA (2007) Biosens Bioelectron 22:1131–1137
24. Kyprianou D, Guerreiro AR, Chianella I, Piletska EV, Fowler SA, Karim K, Whitcombe MJ, Turner APF, Piletsky SA (2009) Biosens Bioelectron 24:1365–1371
25. Hayden O, Lieberzeit P, Blaas D, Dickert FL (2006) Adv Funct Mater 16:1269–1278
26. Miyata T, Jige M, Nakaminami T, Uragami T (2006) Proc Natl Acad Sci USA 103:1190–1193
27. Rampey AM, Umpleby RJ, Rushton GT, Iseman JC, Shah RN, Shimizu KD (2004) Anal Chem 76:1123–1133
28. Ebadi A, Mohammadzadeh JSS, Khudiev A (2009) Adsorption 15:65–73
29. Dickert FL, Haunschild A, Kuschow V, Reif M, Stathopulos H (1996) Anal Chem 68:1058–1061
30. Dickert FL, Hayden O (2002) Anal Chem 74:1302–1306
31. Schwefel D, Maierhofer C, Beck JG, Seeberger S, Diederichs K, Möller HM, Welte W, Wittmann V (2010) J Am Chem Soc 132:8704–8719
32. Lieberzeit PA, Schirk C, Glanznig G, Gazda-Miarecka S, Bindeus R, Nannen H, Kauling J, Dickert FL (2004) Superlatt Microstruct 36:133–142
33. Dickert FL, Hayden O, Lieberzeit P, Palfinger C, Pickert D, Wolff U, Scholl G (2003) Sens Actuators B 95:20–24
34. Lucklum R, Behling C, Hauptmann P (1999) Anal Chem 71:2488–2496
35. Peters T Jr (1985) Adv Protein Chem 37:161–245
36. Schirhagl R, Podlipna D, Lieberzeit PA, Dickert FL (2010) Chem Commun 3128-3130
37. Jenik M, Schirhagl R, Schirk C, Hayden O, Lieberzeit P, Blaas D, Paul G, Dickert FL (2009) Anal Chem 81:5320–5326
38. Dickert FL, Hayden O, Lieberzeit P, Haderspoeck C, Bindeus R, Palfinger C, Wirl B (2003) Synth Met 138:65–69